IEEE Access
Multidisciplinary ⋮ Rapid Review ⋮ Open Access Journal

Received June 18, 2020, accepted July 1, 2020, date of publication July 21, 2020, date of current version September 17, 2020.

Digital Object Identifier 10.1109/ACCESS.2020.3011022

Capacity of Unmanned Aerial Vehicle Assisted Data Collection in Wireless Sensor Networks

ZHIQING WEI[1], (Member, IEEE), QIAN CHEN[1], SHUHANG LIU[2], AND HUICI WU[1], (Member, IEEE)

[1]Key Laboratory of Universal Wireless Communications, Ministry of Education, Beijing University of Posts and Telecommunications, Beijing 100876, China
[2]China Tower, Beijing 100143, China

Corresponding author: Huici Wu (dailywu@bupt.edu.cn)

This work was supported in part by the Beijing Natural Science Foundation under Grant L192031, and in part by the National Natural Science Foundation of China under Grant 61901051.

ABSTRACT Due to the flexibility and mobility, unmanned aerial vehicle (UAV) can work as a movable sink to receive the data collected by sensors in wireless sensor networks (WSNs). This paper analyzes the capacity of UAV assisted data collection in WSNs, which provides a guideline for the parameters optimization of data collection in the presence of UAVs. In this paper, the service area of UAVs covers the area where sensors are distributed. The charging points for UAVs are placed around the service area, which provides energy supply for UAVs. The charging point is the starting and ending point of a UAV's trajectory. The service area is partitioned into multiple service cells. UAVs traverse these service cells to receive the data collected by the sensors in the service cells. The per-node capacity and average execution time of UAVs are used as two metrics to measure the performance of data collection in WSN. The upper and lower bounds of per-node capacity are derived respectively. It is discovered that the number of UAVs, the number of service cells and the trajectories of UAVs affect the per-node capacity of WSN. The per-node capacity can be optimized by adjusting the numbers of UAVs and service cells. Two path planning algorithms of UAVs are designed. With path planning, the per-node capacity is optimized to be closer to the upper bound, which achieves highly efficient data collection. The simulation results verify the correctness of the derived results.

INDEX TERMS Wireless sensor networks, unmanned aerial vehicle, data collection, capacity analysis, path planning, trajectory optimization.

I. INTRODUCTION

Wireless sensor networks (WSNs) are widely applied in intelligent transportation, forest monitoring, ocean monitoring, etc. The number of sensors in the world will increase dramatically in the future. Under this situation, highly efficient collection of sensing data will be crucial. However, there exist significant challenges for the collection of sensing data in some areas lacking the coverage of communication infrastructures, such as ocean, island and forest [1].

Moreover, for large-scale WSNs, the data collection faces a great challenge. Since the number of sensors in WSN is large, the probability of network topology change or network failure is correspondingly large. Compared with small-scale WSNs, the realization of multi-hop information transfer and self-adaptive functions in the large-scale WSNs are more difficult, the data transmission delay is larger and the network lifetime is shorter [2]. The highly efficient data collection method is necessary for large-scale WSNs and the WSNs without communication infrastructures.

Due to the advantages of flexibility and easy deployment, unmanned aerial vehicle (UAV) can work as a movable sink to receive the data collected by sensors in WSNs. UAV assisted data collection in WSNs can be realized in the absence of infrastructure coverage. Besides, the number of hops of data transmission can be reduced to enhance the survivability of WSNs [3], [4], [5]. The network capacity can be improved when exploiting the mobility of UAVs [6], [7]. Moreover, UAV can monitor multiple moving targets [8], locate nodes distributed randomly in the networks [9], and even temporarily replace the faulty nodes of the networks to achieve the functions of self-organization and adaption, which makes the networks more robust [1].

To improve the capacity of UAV assisted data collection in WSNs, the networking schemes of WSNs and the trajectories of UAVs need to be designed. For example, the

The associate editor coordinating the review of this manuscript and approving it for publication was Zihuai Lin.

clustering, multiple access control and routing schemes of WSNs need to be designed and the height, speed, trajectories, energy supply and spectrum allocation of UAVs need to be optimized. Some literatures have focused on designing the optimal trajectories of UAVs to improve the capacity of data collection. Guo *et al.* in [10] analyzed the performance of air-to-ground (A2G) communication when UAVs are applied to support the ground networks. Gong *et al.* in [11] designed the trajectory of single UAV in a one-dimensional (1-D) network. The data collection interval and the flight speed of UAV are designed using dynamic programming (DP) to reduce the UAV's working time when each energy-constrained sensor could upload a certain amount of data. Xue *et al.* designed the trajectory of single UAV in two-dimensional (2-D) network and three-dimensional (3-D) network in [12] and [13], respectively. They maximized the minimum amount of data collected by single UAV under the premise of constrained energy of UAV. Yang *et al.* in [14] studied the suspension height problem in the trajectories of multiple UAVs to reach the best trade-off of energy consumption between the sensors and UAVs. Liu *et al.* in [4] and Zhang *et al.* in [15] applied deep reinforcement learning to design the trajectories of multiple UAVs in smart cities, such that UAVs could collect more data whereas consuming less energy. Zhang *et al.* in [16] designed the trajectories of UAVs through directional dynamic programming (DDP), which reduced the computational complexity and enabled UAVs to adapt to various terrains. You *et al.* in [17] adopted the angle-dependent rician fading channel instead of the probabilistic line-of-sight (LoS) or non-line-of-sight (NLoS) channel in the study of UAV assisted data collection in WSN. Moreover, 3-D trajectories of multiple UAVs were designed to improve the minimum data rate.

In addition to optimizing the trajectories of UAVs, some studies have improved the capacity of data collection by optimizing the networking schemes of WSNs. Albu-Salih *et al.* in [18] designed the clustering algorithm of sensors. Then, UAVs only collect the data of the cluster head in each cluster. They found the optimal routing using mixed-integer linear programming (MILP) to reduce the number and the working time. According to the locations of sensors, Say *et al.* in [19] classified the sensors into different frames corresponding to different transmission priorities. They designed a routing scheme to make data collection more efficient, prolong the lifetime of WSN, and maximize the throughput of WSN. Ebrahimi *et al.* in [20] clustered the sensors and established the tree-shaped routing structure to make data collection more efficient and minimize the number of hops in data transmission.

Furthermore, the improvement of data collection capacity was studied through the joint optimization of UAVs and WSNs. Zhan *et al.* in [2] and Rao *et al.* in [5] jointly optimized the wake-up scheme of sensors and the trajectories of UAVs whereas [2] aims to reduce the upper bound of energy consumption of sensors and [5] aims to minimize the energy consumption and delay of data transmission simultaneously. Besides, [5] discovered a trade-off between the network lifetime and the delay of data transmission. Hua *et al.* in [21] and Zhan *et al.* in [22] jointly optimized the wake-up scheme of sensors and the trajectories of UAVs to reduce the time of UAVs' mission execution under the constraint that all the sensors could transmit a certain amount of data with constrained energy. Liu *et al.* in [23] set sensors to different levels of backbone sampling points and designed the corresponding trajectories of UAVs to reduce the energy consumption and redundancy of collected data. Ghorbel *et al.* in [24] partitioned the coverage area of UAVs and found the best locations of data sampling points. Then, the corresponding trajectories of UAVs are designed to minimize the energy consumption of sensors and UAVs. According to the distribution of sensors, Bushnaq *et al.* in [25] determined the appropriate number of data sampling points and designed the corresponding trajectories of UAVs to reach the best trade-off between the suspension time and flight time of UAVs such that the working time of each UAV was minimized.

In the research of UAV-assisted data collection in WSNs, various optimization objectives can be established. Based on these optimization objectives, the corresponding trajectories of UAVs and networking schemes of WSN can be designed. Considering that the capacity analysis is not comprehensive enough, we set up a new optimization objective, i.e. capacity optimization, which is different from the related works. This paper aims to analyze the capacity of UAV assisted data collection in WSNs. Then, the trajectories of UAVs are designed with improving the capacity as the primary optimization objective function, the execution time and energy consumption of UAVs are thus confirmed. In Section V, the impact of path planning algorithms on capacity is analyzed, which is also different from the related works. Both single-UAV and multi-UAV scenarios are considered. To solve this problem, we assume that each UAV has just enough energy to fly along a preset trajectory, receive the data collected by the sensors and return to the starting point. Then, the amount of data collected during a flight of UAV is equal to the amount of data accumulated by the sensors during the interval between two adjacent flights. According to this analysis, we can derive the per-node capacity. By analyzing the upper and lower bounds of the length of UAV's trajectory, the upper and lower bounds of per-node capacity in single-UAV and multi-UAV scenarios can be derived. Two path planning algorithms are adopted to shorten the length of UAV's trajectory, such that the per-node capacity is optimized to be closer to the upper bound, which achieves highly efficient data collection. The simulation results verify the correctness of the derived per-node capacity. It is noted that compared with the conference version [33], this paper derives the upper and lower bounds of the capacity of data collection. Since the length of UAVs' trajectories has an impact on the capacity, two path planning algorithms with different complexity are proposed for UAVs, such that the capacity of UAV assisted data collection is improved.

The structure of this paper is arranged as follows. Section II introduces the system model. Section III derives the upper and lower bounds of the per-node capacity in single-UAV and multi-UAV scenarios. Section IV designs the path planning algorithms to generate a short trajectory for each UAV. Section V provides the simulation results, which verifies the theoretical results. Section VI summarizes this paper.

II. SYSTEM MODEL

The service area of UAVs covers the area where sensors are distributed. The service area is partitioned into multiple service cells. The charging points for UAVs are placed around the service area, which provides energy supply for UAVs. The charging point is the starting and ending point of a UAV's trajectory.

Without loss of generality, the shape of the service area is assumed to be square. As illustrated in Fig. 1, m sensors are deployed in the service area with side length L. The service area is partitioned into n^2 service cells with side length $\frac{L}{n}$. $4(n+1)$ charging points surrounding the service area act as the starting and ending points of UAVs. The service area of UAVs is not smaller than the coverage area of WSN. The coverage area of WSN in the service area of UAVs can be in any shape, such as the irregular area in Fig. 1.

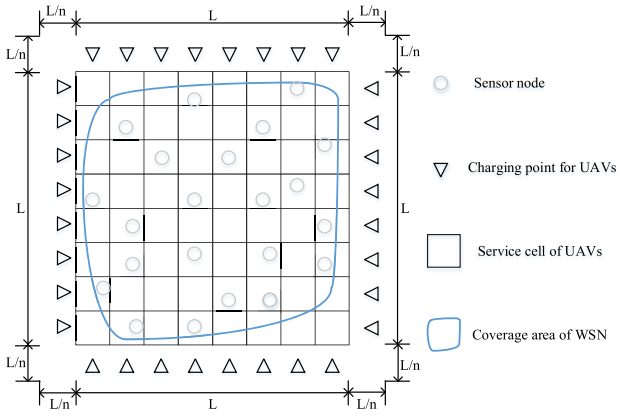

FIGURE 1. The service area, charging points and coverage area of WSN.

A. CHANNEL MODEL

Both LoS and NLoS links are considered for the channel between UAV and ground sensor, i.e., air-to-ground (A2G) channel. The probabilities of A2G channel being LoS and NLoS are denoted as P_{L} and P_{NL}, respectively. Applying the Sigmod model in [26], [27], P_{L} and P_{NL} are expressed as follows.

$$P_{\mathrm{L}} = \frac{1}{1 + a\exp[-b-(\theta-a)]}, \tag{1}$$

$$P_{\mathrm{NL}} = 1 - P_{\mathrm{L}}, \tag{2}$$

where a and b are environment parameters characterizing the number of obstacles in the A2G channel.

The circular coverage area of UAVs is considered. The minimum radius of the coverage disk of UAVs covering a service cell is

$$R_c = \frac{L}{\sqrt{2}n}. \tag{3}$$

The maximum distance between the UAV and a sensor in the service cell covered by UAV is

$$d_0 = \sqrt{h^2 + R_c^2}, \tag{4}$$

where h is the altitude of UAVs.

The elevation angle θ (in degree) of the UAV to sensor link is thus given by

$$\theta = \frac{180}{\pi}\sin^{-1}(\frac{h}{d_0}). \tag{5}$$

The transmit power of sensors is defined as P_d. The received signal power at UAV is denoted as P_r. Path loss fading is considered whereas small-scale fading is ignored in this paper since it has a small impact on the capacity of UAV assisted data collection. Thus, P_r can be expressed as [27]

$$P_r = \begin{cases} P_d d_0^{-\alpha_e}, & \text{LoS} \\ \eta P_d d_0^{-\alpha_e}, & \text{NLoS}, \end{cases} \tag{6}$$

where η is the additional attenuation factor due to NLoS propagation, and α_e is the A2G channel's path loss exponent.

As a result, the UAV's average received signal-to-noise ratio (SNR) is given by

$$\begin{aligned}\beta &= \frac{P_r}{N} \\ &= \frac{P_{LoS}P_d\sqrt{(h^2+\frac{L^2}{2n^2})^{-\alpha_e}} + \eta P_{NLoS}P_d\sqrt{(h^2+\frac{L^2}{2n^2})^{-\alpha_e}}}{N},\end{aligned} \tag{7}$$

where N is the power of additive white Gaussian noise (AWGN). The capacity of A2G channel is given by

$$C_{re} = W_u \log_2(1+\beta), \tag{8}$$

where W_u is the channel bandwidth of A2G channel.

B. DISTRIBUTION MODEL OF SENSORS

The service cell that does not contain any sensors is called empty service cell. The service cell that contains at least one sensor is called non-empty service cell. The number of non-empty service cells is denoted as n_p. The number of methods that m sensors are deployed in n_p service cells is [28]

$$S_2(m, n_p) = \frac{1}{n_p!}\sum_{k=0}^{n_p}(-1)^k C_{n_p}^k (n_p - k)^m. \tag{9}$$

The probability of the number of non-empty service cells being n_p is formulated as

$$p(n_p) = \frac{S_2(m, n_p)A_{n^2}^{n_p}}{(n^2)^m}, \tag{10}$$

where $A_{n^2}^{n_p}$ is the permutations number.

The expectation of n_p is formulated as

$$E(n_p) = \begin{cases} \sum_{n_p=1}^{m} n_p \cdot p(n_p), & m < n^2, \\ \sum_{n_p=1}^{n^2} n_p \cdot p(n_p), & m \geq n^2. \end{cases} \tag{11}$$

III. PER-NODE CAPACITY AND AVERAGE EXECUTION TIME OF UAVs

In this paper, per-node capacity, denoted by λ, and average execution time of UAVs in one cycle, denoted by T_w, are adopted as two metrics to measure the performance of UAV assisted data collection in WSNs. λ is defined as the maximum amount of data accumulated at each sensor and collected by each UAV per unit time.

In order to comprehensively study the performance of UAV assisted data collection in WSNs, we consider the scenarios of single-UAV and multi-UAV. In single-UAV scenario, UAV needs to receive the data collected by all the sensors in the entire service area as shown in Fig. 2(a). UAV flies along the trajectory denoted by the red line. The scenario where the number of UAVs is at least 2 is called multi-UAV scenario. In multi-UAV scenario, the entire service area is partitioned into several parts. Each UAV needs to receive the data collected by the sensors in its responsible part. Take the multi-UAV scenario with two UAVs as an example, the responsible part of each UAV is shown in Fig. 2(b). The lines in different colors indicate trajectories of different UAVs. It is noted that all the figures of multi-UAV scenario in this paper take two UAVs as an example to make the illustration of figures more concise.

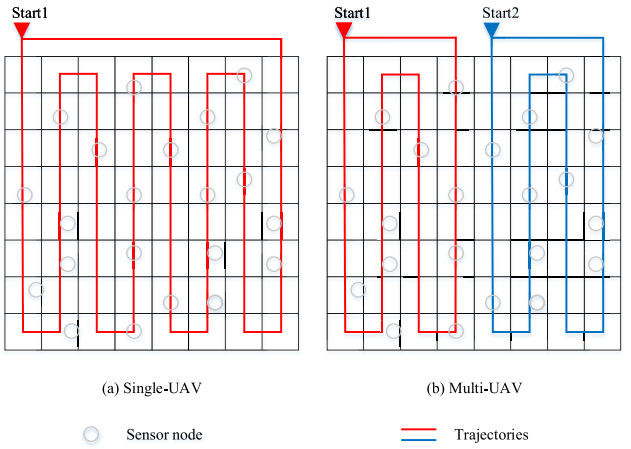

FIGURE 2. The trajectories of UAVs in single-UAV and multi-UAV scenarios to derive the lower bound of capacity.

We regard the sensors in the same service cell as a cluster and select one sensor in the cluster as the cluster head. The cluster head aggregates the data collected by all sensors in the cluster. The UAV can indirectly collect data from all the sensors in the service cell through the cluster heads when UAV passes through the service cells. It is noted that the cluster head does not necessarily lie in the center of the service cell. The design of UAV's trajectory near the cluster head can be found in [29] when UAV communicates with the cluster head. This paper mainly considers the design of UAVs' trajectories among multiple service cells. The UAV starts from a starting point, traverses all the non-empty service cells in turn, and then, returns to the starting point periodically. The UAV continues to the next flight after energy replenishment at the starting point.

A. SINGLE-UAV SCENARIO

In single-UAV scenario, the communication bandwidth that the UAV can use is W. The channel bandwidth of a UAV is

$$W_u = W. \tag{12}$$

To ensure that the UAV can receive all the data collected by the sensors located in the service cell, we set the pause time of UAV in each service cell, denoted by t_s, as the ratio of the total amount of data accumulated by the sensors located in the service cell to the capacity of A2G channel.

$$t_s = \frac{m\lambda_s T_w}{n_p C_{re}}, \tag{13}$$

where T_w is the execution time of UAV in one cycle, λ_s is the per-node capacity.

To maintain the UAV's operation in a complete round-trip, the supplemented energy for UAV at the starting point is

$$E_u = n_p t_s (P_d + P_f) + \frac{S}{v} P_f, \tag{14}$$

where P_f is the power for flight, P_d is the transmit power of sensors, v is the flying speed of UAV, S is the length of UAV's trajectory in one cycle.

Substituting (8), (12) and (13) to (14), the execution time of UAV in one cycle and the per-node capacity can be written as

$$T_w = n_p t_s + \frac{S}{v} = \frac{vE_u + SP_d}{v(P_d + P_f)}, \tag{15}$$

$$\lambda_s = \frac{(vE_u - SP_f)W\log_2(1+\beta)}{mvE_u + mSP_d}. \tag{16}$$

According to (15), T_w is a monotonically increasing function of E_u and S, i.e., the execution time of UAV in one cycle increases as the supplemented energy for UAV at the starting point or the length of UAV's trajectory in one cycle increases. According to (16), λ_s is a monotonically decreasing function of S, i.e., the per-node capacity in single-UAV scenario decreases as the length of UAV's trajectory in one cycle increases.

UAV has the longest trajectory when all service cells contain sensors as shown in Fig. 2(a), which is the algorithm explained in [30]. We can derive the lower bound of per-node capacity in this case.

$$n_p = n^2, \tag{17}$$

$$S = \frac{(n_p + n)L}{n} = (n+1)L. \tag{18}$$

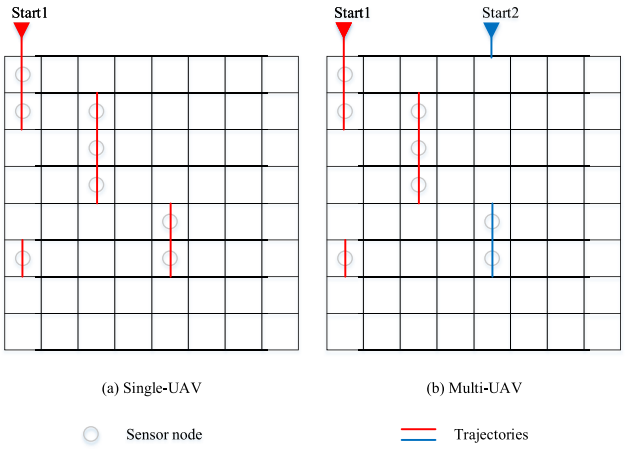

FIGURE 3. The trajectories of UAVs in single-UAV and multi-UAV scenarios to derive the upper bound of capacity.

Substituting (17) and (18) to (16), the lower bound of the per-node capacity in single-UAV scenario is

$$\lambda_{s,l} = \frac{[vE_u - (n+1)LP_f]W\log_2(1+\beta)}{mvE_u + m(n+1)LP_d}. \tag{19}$$

To derive the upper bound of λ_s, the extreme case is considered where UAV only flies over the non-empty service cells as shown in Fig. 3(a).

$$1 \le n_p < n^2, \tag{20}$$

$$S = \frac{(n_p+1)L}{n}. \tag{21}$$

Substituting (21) to (16), the upper bound of the per-node capacity is

$$\lambda_{s,u} = \frac{[vnE_u - (n_p+1)LP_f]W\log_2(1+\beta)}{mvnE_u + m(n_p+1)LP_d}. \tag{22}$$

B. MULTI-UAV SCENARIO

In multi-UAV scenario, each UAV is in charge of part of the service area and occupies half of the frequency band, such that adjacent UAVs do not interfere with each other. The channel bandwidth of each UAV is

$$W_u = \frac{W}{2}. \tag{23}$$

According to the definition of t_s, it can be expressed as

$$t_s = \frac{m\lambda_m T_w}{n_p/uC_{re}}, \tag{24}$$

where u is the number of UAVs, T_w is the average execution time of UAVs in one cycle, λ_m is the per-node capacity.

To maintain the UAVs' operation in a complete round-trip, the average supplemented energy for UAVs at the starting points is

$$E_u = \frac{n_p}{u}t_s(P_d + P_f) + \frac{S}{vu}P_f, \tag{25}$$

where S is the summation of the length of UAVs' trajectories in one cycle.

Substituting (8), (23) and (24) to (25), the average execution time of UAVs in one cycle and the per-node capacity can be written as

$$T_w = \frac{n_p}{u}t_s + \frac{S}{vu} = \frac{vE_u + SP_d}{vu(P_d + P_f)}, \tag{26}$$

$$\lambda_m = \frac{(vuE_u - SP_f)W\log_2(1+\beta)}{2mvE_u + 2mSP_d}. \tag{27}$$

According to (26), T_w is a monotonically decreasing function of u, i.e., the average execution time of UAVs in one cycle decreases as the number of UAVs increases. According to (27), λ_m is a monotonically increasing function of u, i.e., the per-node capacity in multi-UAV scenario increases as the number of UAVs increases.

UAVs have the longest trajectories when all the service cells contain sensors as shown in Fig. 2(b). Substituting (17) and (18) to (27), the lower bound of the per-node capacity in multi-UAV scenario is

$$\lambda_{m,l} = \frac{[vuE_u - (n+1)LP_f]W\log_2(1+\beta)}{2mvE_u + 2m(n+1)LP_d}. \tag{28}$$

To derive the upper bound of λ_m, the extreme case is considered where UAVs only fly over the non-empty service cells as shown in Fig. 3(b).

$$S = \frac{(n_p+u)L}{n}. \tag{29}$$

Substituting (29) to (27), the upper bound of the per-node capacity is

$$\lambda_{m,u} = \frac{[vunE_u - (n_p+u)LP_f]W\log_2(1+\beta)}{2mvnE_u + 2m(n_p+u)LP_d}. \tag{30}$$

IV. IMPACT OF PATH PLANNING ALGORITHMS ON PER-NODE CAPACITY

According to Section III, the length of UAV's trajectory has an impact on the per-node capacity. To find the shortest trajectory covering all the non-empty service cells and return to the starting point, we study the path planning algorithms in the two cases of fixed starting points and adaptive starting points for UAVs in this section.

A. PATH PLANNING ALGORITHMS WITH FIXED STARTING POINTS

In practice, UAVs pass through neither all the service cells nor only the non-empty service cells when the distribution of non-empty service cells is estimated. Thus, the path planning algorithms need to be designed to discover the shortest path to traverse the non-empty service cells.

The path planning algorithm with fixed starting points is summarized in Algorithm 1. With the first and last columns in the service area as the starting column col_1 and ending column col_2 of UAVs, UAVs traverse each column in turn between col_1 and col_2. The starting point of each UAV is fixed in front of the UAV's starting column.

Algorithm 1 The path planning algorithm with fixed starting points.

1: $j = col_1; P_1 = 0;$
2: **while** $j \leq col_2$ **do**
3: **if** $\text{sum}(C_j) \geq 1$ **then**
4: $index = \text{find}(C_j);$
5: **else**
6: $index = 1;$
7: **end if**
8: **if** $j + 1 \leq n$ **then**
9: **if** $\text{sum}(C_{j+1}) \geq 1$ **then**
10: $index\_\text{next} = \text{find}(C_{j+1});$
11: **else**
12: $index\_\text{next} = 1;$
13: **end if**
14: **else**
15: $index\_\text{next} = index;$
16: **end if**
17: $i = max(index, index\_\text{next});$
18: $P_1 = P_1 + i \times 2;$
19: $j = j + 2;$
20: **end while**
21: $S = (P_1 + col_2 - col_1 + 1) \times \frac{L}{n};$

In the initialization stage of Algorithm 1, $j = col_1$ means that UAVs start from the col_1-th column and $P_1 = 0$ means that the number of service cells passed by UAVs is zero at the beginning. In the 3-rd line of Algorithm 1, $\text{sum}(C_j) > 0$ means that there is at least one non-empty service cell in the j-th column. In the 4-th and 10-th lines of Algorithm 1, *index* and *index*_next record the maximal row numbers of non-empty service cells in the j-th and $(j + 1)$-th columns respectively. The larger one between *index* and *index*_next is denoted by i.

The two adjacent columns can be a back and forth as shown in Fig. 4. UAVs need to start from $C_{1,j}$, farthest to $C_{i,j}$, the next is $C_{i,j+1}$, back to $C_{1,j+1}$, and the next round start from the $C_{1,j+2}$. Repeat the above rules until UAVs fly over the last column col_2.

The trajectories in single-UAV and multi-UAV scenarios with Algorithm 1 are shown in Fig. 5(a) and Fig. 5(b) respectively.

In multi-UAV scenario, the service area of each UAV is smaller compared with single-UAV scenario. The summation of the length of UAVs' trajectories in one cycle, denoted by S, are the same for single-UAV and multi-UAV scenarios with Algorithm 1. The starting point of each UAV is fixed.

B. PATH PLANNING ALGORITHMS WITH ADAPTIVE STARTING POINTS

There is still redundancy in the trajectories of UAVs when the starting points are fixed. We choose the ant colony algorithm [31] for path planning so that UAVs can choose the starting points adaptively according to the distribution of non-empty service cells.

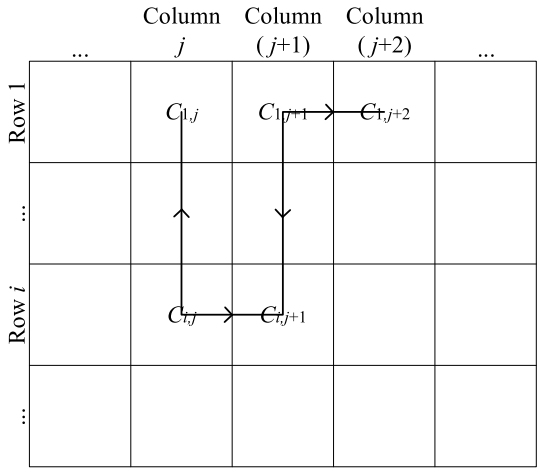

FIGURE 4. A back and forth movement of UAV with Algorithm 1.

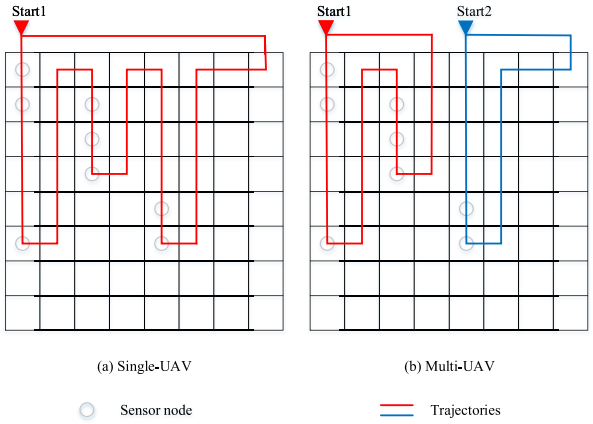

FIGURE 5. The trajectories of UAVs with Algorithm 1.

Ant colony algorithm belongs to the heuristic algorithms. The heuristic algorithms simulate some natural phenomena and obtain a feasible solution that is not necessarily the optimal solution after a certain number of iterations. Ant colony algorithm simulates the natural phenomena of ant-foraging. The ants always tend to choose the shortest path between the food and the nest no matter how many obstacles in the path, because ants will release pheromones along the way, such that more and more ants per unit of time will pass through the shorter path where more pheromones will be accumulated. Ants always tend to choose the path with the most pheromones, which creates positive feedback to choose the shortest path [31].

UAVs can only move between the adjacent service cells, which means that UAVs can not slash in the 2D plane. The Manhattan distance $d_{i,j}$ is defined as the minimum number of service cells to pass from service cell i to service cell j [32]. For example, $d_{i,j}$ is 1 when service cell i and service cell j are two adjacent service cells.

The visibility between service cell i and service cell j is defined as

$$\eta_{i,j} = \frac{1}{d_{i,j}}. \tag{31}$$

All the pheromone concentrations $c_{i,j}^0$ between any two service cells are initialized to 1 before the iteration begins. After each iteration, the pheromone concentrations need to be updated to

$$c_{i,j}^{k+1} = (1-\rho)c_{i,j}^k + \Delta c_{i,j}^k, \tag{32}$$

where ρ is the pheromone concentration volatilization coefficient.

The increment of pheromone concentration released by the ant A and all ants between service cell i and service cell j in the k-th iteration can be formulated as follows according to the principle of ant colony algorithm [31]

$$\Delta c_{i,j}^k(A) = \begin{cases} \frac{Q}{d_A}, & i_A \to j_A \\ 0, & \text{otherwise}, \end{cases} \tag{33}$$

$$\Delta c_{i,j}^k = \sum_{A=1}^{n_{ant}} \Delta c_{i,j}^k(A), \tag{34}$$

where Q is a constant that represents the total amount of pheromone concentration released by one ant in one cycle, d_A is the number of service cells that ant A passes through in one cycle, and $i_A \to j_A$ represents that ant A chooses to walk from service cell i to service cell j in this cycle, n_{ant} is the total number of ants in each iteration.

The probability that ant A walks from service cell i to service cell j in the k-th iteration is formulated as follows according to the principle of ant colony algorithm [31]

$$p_{i,j}^k(A) = \frac{|c_{i,j}^k(A)|^\alpha \cdot |\eta_{i,j}|^\beta}{\sum_{j=\in r_A} |c_{i,j}^k(A)|^\alpha \cdot |\eta_{i,j}|^\beta}. \tag{35}$$

The pheromone concentration heuristic factor is α. The ant will have a larger probability to select the path that has been passed before when α is larger. The search range of the ants is smaller when the randomness of the search path is weaker. The ants will no longer consider pheromone concentration levels if $\alpha = 0$.

The path heuristic factor is β. The ants are easier to select the locally shorter path when β is larger. The set $\mathbb{R}_A$ represents the set of the non-empty service cells that ant A has not passed. The ant colony algorithm for path planning is summarized in Algorithm 2.

In the 1-st line of Algorithm 2, the value of K is set before the algorithm begins to iterate. Algorithm 2 can obtain a feasible solution that is not necessarily the optimal solution after K iterations. In the 11-th line of Algorithm 2, the purpose is to find the minimal number of service cells passed by from the paths of all the ants in the k-th iteration. In the 14-th line of Algorithm 2, the purpose is to find the minimal number of service cells passed by from the paths of all the iterations. In the 16-th line of Algorithm 2, P_{back} is the minimal number of service cells that need to pass from service cell to the starting point.

Algorithm 2 The ant colony based path planning algorithm.

1: **for** $k = 1; k \le K; k = k + 1$ **do**
2: **for** $A = 1; A \le n_{ant}; A = A + 1$ **do**
3: Ant A randomly selects one of non-empty service cells to start walking;
4: **for** $n_c = 1; n_c \le n_p; n_c = n_c + 1$ **do**
5: Find the set of the non-empty service cells that ant A has not passed, which is denoted by $\mathbb{R}_A$;
6: Calculate $p_{i,j}^k(A)$ as shown in (35);
7: Select the service cell with the highest $p_{i,j}^k(A)$ as the next step of the path;
8: **end for**
9: Calculate the number of service cells passed by ant A in the k-th iteration P_A^k;
10: **end for**
11: $P^k = \min(P_A^k)$;
12: Update $c_{i,j}^{k+1}$ as shown in (32);
13: **end for**
14: $P_2 = \min(P^k)$;
15: Find the nearest charging point as the starting point;
16: $S = (P_2 + 2 \times P_{back}) \times \frac{L}{n}$;

The trajectories in single-UAV and multi-UAV scenarios with Algorithm 2 are shown in Fig. 6(a) and Fig. 6(b) respectively.

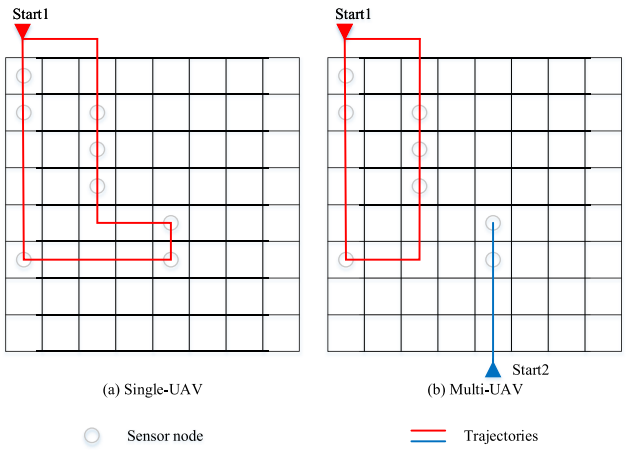

FIGURE 6. The trajectories of UAVs with Algorithm 2.

The summation of the length of UAVs' trajectories in one cycle S in multi-UAV scenario obtained with Algorithm 2 is larger than that in single-UAV scenario, which is different from the case with Algorithm 1. In Algorithm 2, the length of UAVs' trajectories is related to the distribution of sensors and the number of UAVs. The most suitable charging point can be selected as the starting point for each UAV automatically.

V. EXPERIMENTAL RESULTS AND ANALYSIS

In this section, we verify the theoretical results of the number of non-empty service cells and the bounds of per-node capacity by simulation results. Through the method of control variables, we study the relationship between some dependent

variables and independent variables. The dependent variables we studied include the number of non-empty service cells, the per-node capacity, and the average execution time of UAVs. The independent variables we studied include the number of sensors, service cells and UAVs. The values of key simulation parameters are shown in Table 1. Detailed description of figures and analysis are given as follows.

TABLE 1. The parameters in simulation.

Notation	Value	Notation	Value	Notation	Value
L	400 m	α_e	1.2	v	8 m/s
h	20 m	η	0.3	E_u	5 kJ
a	11.95	N	0.5	P_f	2 J
b	0.136	W	1000	P_d	4 J

The theoretical results of the number of non-empty service cells are verified by Monte Carlo simulation in Fig. 7 and Fig. 8. According to Fig. 7, the number of non-empty service cells is approximately equal to the number of sensors. According to Fig. 8, the number of non-empty service cells can hardly be affected by the number of service cells when n is large, i.e., the probability that multiple sensors are in the same service cell is almost zero when n is large.

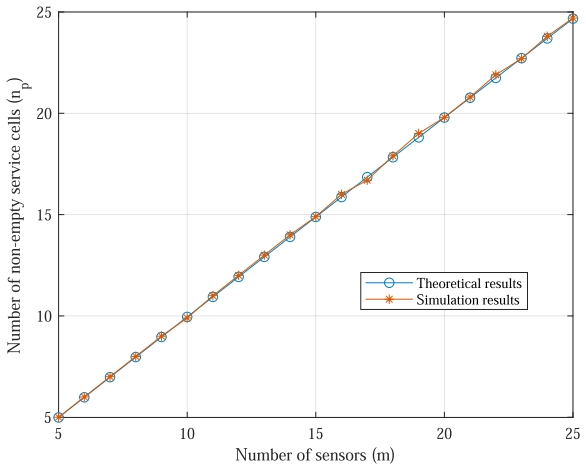

FIGURE 7. The relationship between number of non-empty service cells n_p and number of sensors m with $n = 30$.

The relationship between the per-node capacity and the number of sensors in single-UAV and multi-UAV scenarios are analyzed and compared in Fig. 9 and Fig. 10. The relationship between the per-node capacity and the number of service cells in single-UAV and multi-UAV scenarios are compared and illustrated in Fig. 11 and Fig. 12. The simulation results of the per-node capacity are obtained with Algorithm 1 and Algorithm 2 respectively. The upper and lower bounds of the per-node capacity are obtained from the derivation. According to Fig. 9, Fig. 10, Fig. 11 and Fig. 12, the simulation results of per-node capacity with Algorithm 1 and Algorithm 2 are always between the upper and lower bounds of per-node capacity, which verifies the superiority of two path planning algorithms over the algorithm in [30] and the correctness of derived upper and lower bounds of per-node

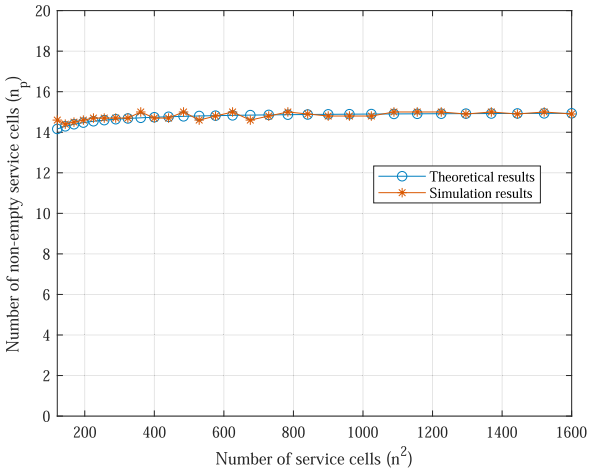

FIGURE 8. The relationship between number of non-empty service cells n_p and number of service cells n^2 with $m = 15$.

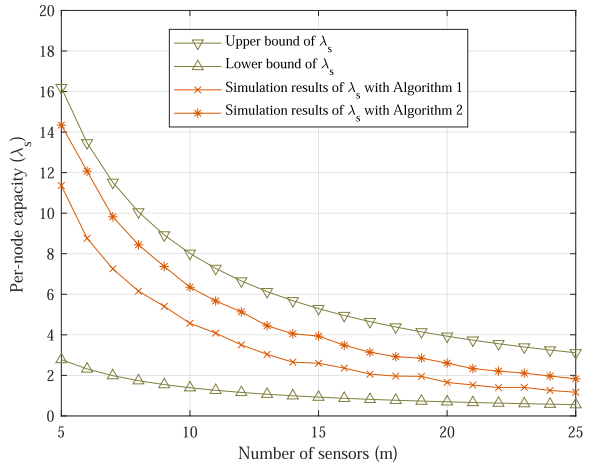

FIGURE 9. The relationship between per-node capacity λ_s and number of sensors m in single-UAV scenario with $n = 30$.

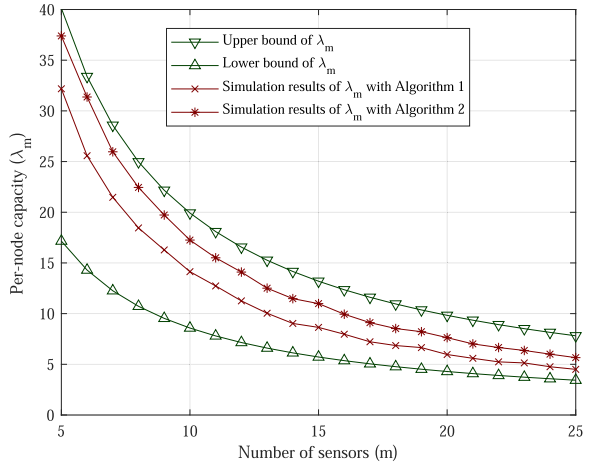

FIGURE 10. The relationship between per-node capacity λ_m and number of sensors m in multi-UAV scenario with $n = 30$ and $u = 10$.

capacity. The per-node capacity obtained with Algorithm 2 are always larger than that with Algorithm 1. As shown in Fig. 9 and Fig. 10, the per-node capacity decreases when the number of sensors increases with a fixed number of service

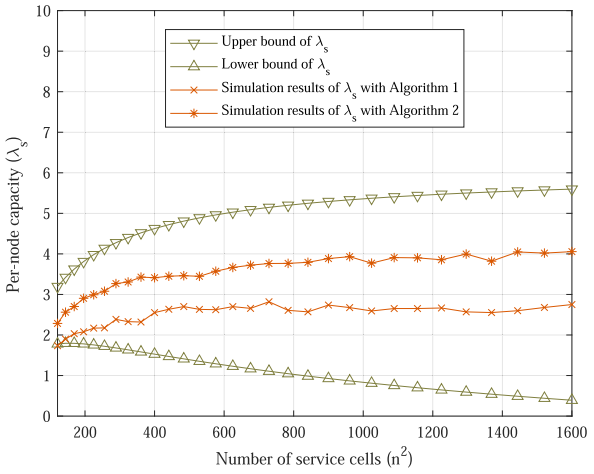

FIGURE 11. The relationship between per-node capacity λ_s and number of service cells n^2 in single-UAV scenario with $m = 15$.

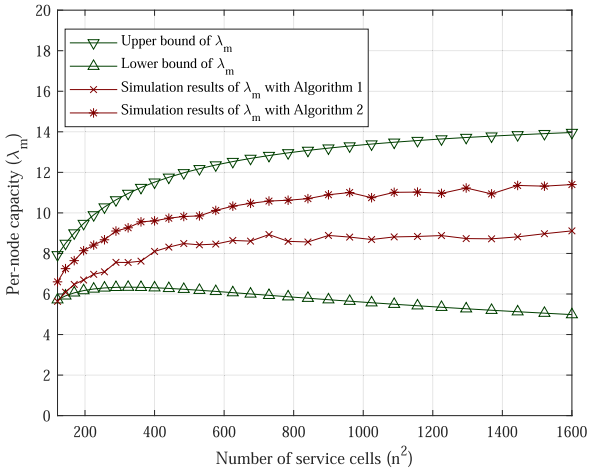

FIGURE 12. The relationship between per-node capacity λ_m and number of service cells n^2 in multi-UAV scenario with $m = 15$ and $u = 10$.

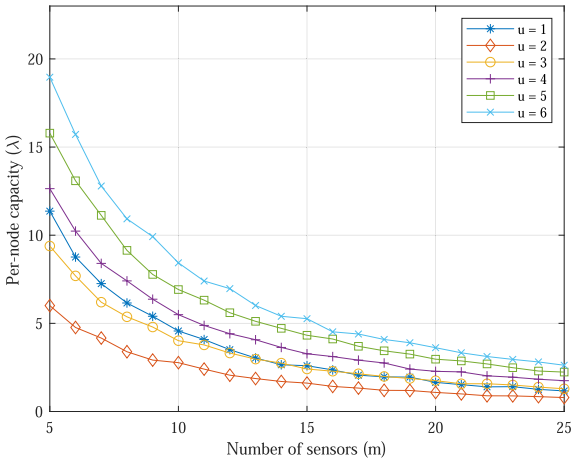

FIGURE 13. The relationship between per-node capacity λ and number of sensors m with Algorithm 1 with $n = 30$.

cells. In Fig. 11 and Fig. 12, the per-node capacity increases as the number of service cells increases when n is small, the per-node capacity can hardly be affected by the number of service cells when n is large.

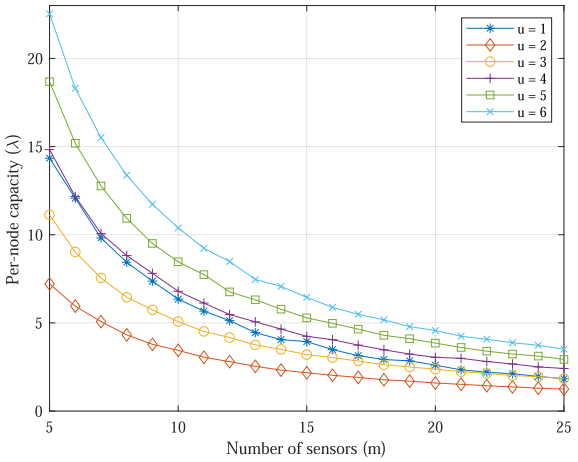

FIGURE 14. The relationship between per-node capacity λ and number of sensors m with Algorithm 2 with $n = 30$.

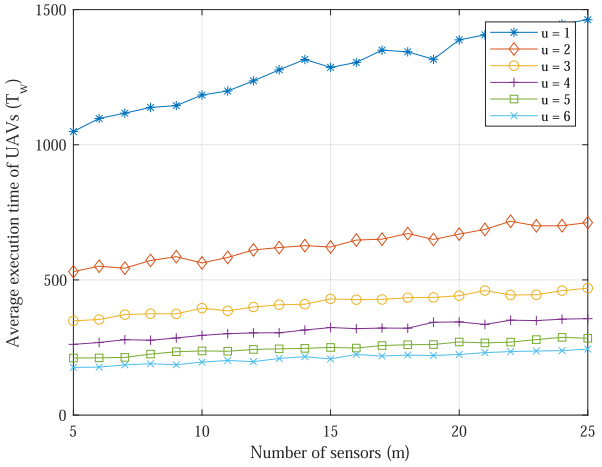

FIGURE 15. The relationship between average execution time of UAVs in one cycle T_w and number of sensors m with Algorithm 1 with $n = 30$.

In actual application, the service area is usually partitioned into an appropriate number of service cells according to the number of available UAVs and the distribution of sensors. The length of UAVs' trajectories will be large when the number of service cells is not large enough, which will reduce the per-node capacity of data collection in WSNs. Therefore, the high value of per-node capacity can be obtained by adjusting the value of the number of service cells.

The relationship between the per-node capacity and the number of UAVs with Algorithm 1 and Algorithm 2 are shown in Fig. 13 and Fig. 14. It is discovered that the per-node capacity changes as the number of UAVs changes. The per-node capacity is the smallest when the number of UAVs is 2. The per-node capacity in multi-UAV scenario is smaller than that in single-UAV scenario when the number of UAVs is not larger than 3. We explain this phenomenon as follows. The per-node capacity increases since multiple UAVs operate simultaneously. The per-node capacity decreases since the bandwidth of each UAV is reduced by half. The increment does not compensate for the decrement when the number of UAVs is not larger than 3. The per-node capacity in multi-UAV scenario is larger than that in single-UAV scenario

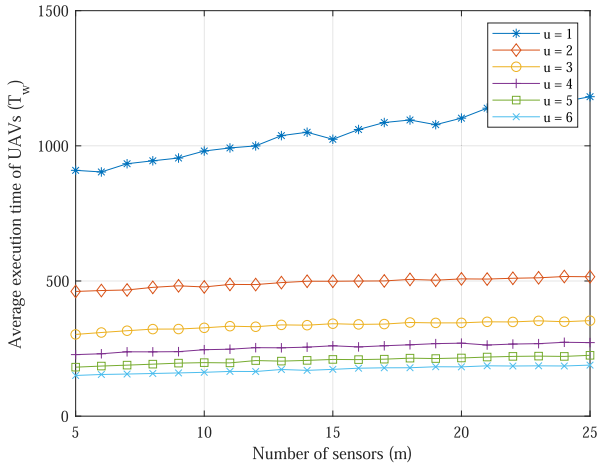

FIGURE 16. The relationship between average execution time of UAVs in one cycle T_W and number of sensors m with Algorithm 2 with $n = 30$.

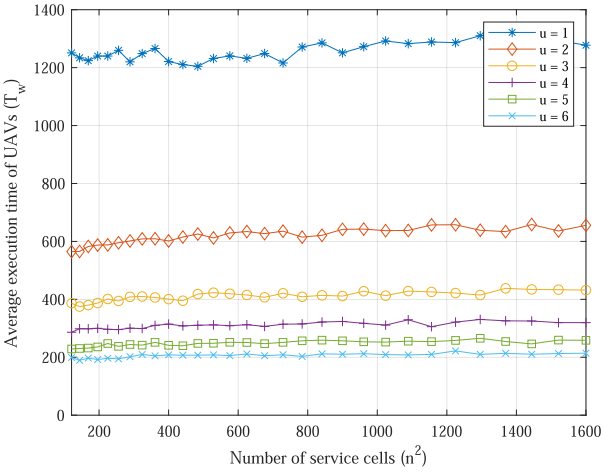

FIGURE 17. The relationship between average execution time of UAVs in one cycle T_W and number of service cells n^2 with Algorithm 1 with $m = 15$.

when the number of UAVs is larger than 3, which is due to the fact that the increment of per-node capacity exceeds the decrement of per-node capacity. Therefore, the high value of per-node capacity can be obtained by adjusting the number of UAVs and bandwidth of the communication channel.

The relationship between the average execution time of UAVs and the number of sensors with Algorithm 1 and Algorithm 2 are shown in Fig. 15 and Fig. 16. The relationship between the average execution time of UAVs and the number of service cells with Algorithm 1 and Algorithm 2 are shown in Fig. 17 and Fig. 18. As illustrated in Fig. 15, Fig. 16, Fig. 17 and Fig. 18, the average execution time of UAVs in one cycle significantly decreases in multi-UAV scenario compared to the scenario of single-UAV. The average execution time of UAVs with Algorithm 2 is always smaller than that with Algorithm 1. Regardless of Algorithm 1 or Algorithm 2, the average execution time of UAVs decreases as the number of UAVs increases. As the number of UAVs continues to increase, the average execution time of UAVs decreases to a certain value and does not continue to decrease. The average execution time of UAVs increases as the number of sensors

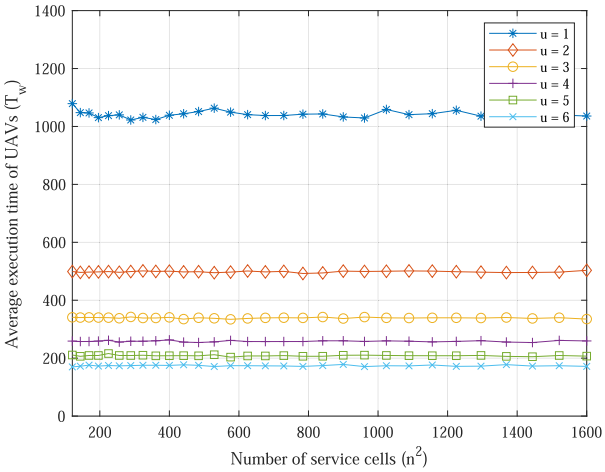

FIGURE 18. The relationship between average execution time of UAVs in one cycle T_W and number of service cells n^2 with Algorithm 2 with $m = 15$.

increases. The average execution time of UAVs is almost unchanged as the number of service cells changes.

VI. CONCLUSION

This paper studies the capacity of UAV assisted data collection in WSNs. The per-node capacity and the average execution time of UAVs are derived in the scenarios of single-UAV and multi-UAV. Two path planning algorithms for UAVs are designed in the scenarios of single-UAV and multi-UAV. The theoretical analyses are verified by the simulation results. The simulation results reveal that Algorithm 2 performs better than Algorithm 1. Compared to Algorithm 1, Algorithm 2 can achieve the per-node capacity closer to its theoretical upper bound within a shorter average execution time of UAVs in one cycle. However, Algorithm 1 has a much lower complexity compared with Algorithm 2. A higher value of the per-node capacity can be obtained by adjusting the number of service cells and UAVs. The per-node capacity increases as the number of UAVs increases. The average execution time of UAVs in one cycle decreases significantly as the number of UAVs increases.

ACKNOWLEDGMENT

This article was presented in part at the IEEE 87th Vehicular Technology Conference [33].

REFERENCES

[1] J. Ueyama, H. Freitas, B. S. Faical, G. P. R. Filho, P. Fini, G. Pessin, P. H. Gomes, and L. A. Villas, "Exploiting the use of unmanned aerial vehicles to provide resilience in wireless sensor networks," *IEEE Commun. Mag.*, vol. 52, no. 12, pp. 81–87, Dec. 2014.

[2] C. Zhan, Y. Zeng, and R. Zhang, "Energy-efficient data collection in UAV enabled wireless sensor network," *IEEE Wireless Commun. Lett.*, vol. 7, no. 3, pp. 328–331, Jun. 2018.

[3] Z. M. Fadlullah, D. Takaishi, H. Nishiyama, N. Kato, and R. Miura, "A dynamic trajectory control algorithm for improving the communication throughput and delay in UAV-aided networks," *IEEE Netw.*, vol. 30, no. 1, pp. 100–105, Jan. 2016.

[4] C. H. Liu, Z. Chen, and Y. Zhan, "Energy-efficient distributed mobile crowd sensing: A deep learning approach," *IEEE J. Sel. Areas Commun.*, vol. 37, no. 6, pp. 1262–1276, Jun. 2019.

[5] J. Rao and S. Biswas, "Data harvesting in sensor networks using mobile sinks," *IEEE Wireless Commun.*, vol. 15, no. 6, pp. 63–70, Dec. 2008.
[6] Z. Wei, Z. Feng, H. Zhou, L. Wang, and H. Wu, "Capacity and delay of unmanned aerial vehicle networks with mobility," *IEEE Internet Things J.*, vol. 6, no. 2, pp. 1640–1653, Apr. 2019.
[7] Z. Wei, H. Wu, S. Huang, and Z. Feng, "Scaling laws of unmanned aerial vehicle network with mobility pattern information," *IEEE Commun. Lett.*, vol. 21, no. 6, pp. 1389–1392, Jun. 2017.
[8] J. Gu, T. Su, Q. Wang, X. Du, and M. Guizani, "Multiple moving targets surveillance based on a cooperative network for multi-UAV," *IEEE Commun. Mag.*, vol. 56, no. 4, pp. 82–89, Apr. 2018.
[9] T. Yu, X. Wang, J. Jin, and K. McIsaac, "Cloud-orchestrated physical topology discovery of large-scale IoT systems using UAVs," *IEEE Trans. Ind. Informat.*, vol. 14, no. 5, pp. 2261–2270, May 2018.
[10] Z. Guo, Z. Wei, Z. Feng, and N. Fan, "Coverage probability of multiple UAVs supported ground network," *Electron. Lett.*, vol. 53, no. 13, pp. 885–887, Jun. 2017.
[11] J. Gong, T.-H. Chang, C. Shen, and X. Chen, "Flight time minimization of UAV for data collection over wireless sensor networks," *IEEE J. Sel. Areas Commun.*, vol. 36, no. 9, pp. 1942–1954, Sep. 2018.
[12] Z. Xue, J. Wang, G. Ding, H. Zhou, and Q. Wu, "Cooperative data dissemination in air-ground integrated networks," *IEEE Wireless Commun. Lett.*, vol. 8, no. 1, pp. 209–212, Feb. 2019.
[13] Z. Xue, J. Wang, G. Ding, H. Zhou, and Q. Wu, "Maximization of data dissemination in UAV-supported Internet of Things," *IEEE Wireless Commun. Lett.*, vol. 8, no. 1, pp. 185–188, Feb. 2019.
[14] D. Yang, Q. Wu, Y. Zeng, and R. Zhang, "Energy tradeoff in ground-to-UAV communication via trajectory design," *IEEE Trans. Veh. Technol.*, vol. 67, no. 7, pp. 6721–6726, Jul. 2018.
[15] B. Zhang, C. H. Liu, J. Tang, Z. Xu, J. Ma, and W. Wang, "Learning-based energy-efficient data collection by unmanned vehicles in smart cities," *IEEE Trans. Ind. Informat.*, vol. 14, no. 4, pp. 1666–1676, Apr. 2018.
[16] Z. Zhang, Q. Wu, B. Zhang, X. Yi, and Y. Tang, "UAV flight strategy algorithm based on dynamic programming," *J. Syst. Eng. Electron.*, vol. 29, no. 6, pp. 1293–1299, Dec. 2018.
[17] C. You and R. Zhang, "3D trajectory optimization in Rician fading for UAV-enabled data harvesting," *IEEE Trans. Wireless Commun.*, vol. 18, no. 6, pp. 3192–3207, Jun. 2019.
[18] A. T. Albu-Salih and S. A. H. Seno, "Energy-efficient data gathering framework-based clustering via multiple UAVs in deadline-based WSN applications," *IEEE Access*, vol. 6, pp. 72275–72286, Nov. 2018.
[19] S. Say, H. Inata, J. Liu, and S. Shimamoto, "Priority-based data gathering framework in UAV-assisted wireless sensor networks," *IEEE Sensors J.*, vol. 16, no. 14, pp. 5785–5794, Jul. 2016.
[20] D. Ebrahimi, S. Sharafeddine, P.-H. Ho, and C. Assi, "UAV-aided projection-based compressive data gathering in wireless sensor networks," *IEEE Internet Things J.*, vol. 6, no. 2, pp. 1893–1905, Apr. 2019.
[21] M. Hua, Y. Wang, Z. Zhang, C. Li, Y. Huang, and L. Yang, "Power-efficient communication in UAV-aided wireless sensor networks," *IEEE Commun. Lett.*, vol. 22, no. 6, pp. 1264–1267, Jun. 2018.
[22] C. Zhan and Y. Zeng, "Completion time minimization for multi-UAV-enabled data collection," *IEEE Trans. Wireless Commun.*, vol. 18, no. 10, pp. 4859–4872, Oct. 2019.
[23] X. Liu, Y. Liu, N. Zhang, W. Wu, and A. Liu, "Optimizing trajectory of unmanned aerial vehicles for efficient data acquisition: A matrix completion approach," *IEEE Internet Things J.*, vol. 6, no. 2, pp. 1829–1840, Apr. 2019.
[24] M. B. Ghorbel, D. Rodriguez-Duarte, H. Ghazzai, M. J. Hossain, and H. Menouar, "Joint position and travel path optimization for energy efficient wireless data gathering using unmanned aerial vehicles," *IEEE Trans. Veh. Technol.*, vol. 68, no. 3, pp. 2165–2175, Mar. 2019.
[25] O. M. Bushnaq, A. Celik, H. Elsawy, M.-S. Alouini, and T. Y. Al-Naffouri, "Aeronautical data aggregation and field estimation in IoT networks: Hovering and traveling time dilemma of UAVs," *IEEE Trans. Wireless Commun.*, vol. 18, no. 10, pp. 4620–4635, Oct. 2019.
[26] A. Al-Hourani, S. Kandeepan, and S. Lardner, "Optimal LAP altitude for maximum coverage," *IEEE Wireless Commun. Lett.*, vol. 3, no. 6, pp. 569–572, Dec. 2014.
[27] J. Holis and P. Pechac, "Elevation dependent shadowing model for mobile communications via high altitude platforms in built-up areas," *IEEE Trans. Antennas Propag.*, vol. 56, no. 4, pp. 1078–1084, Apr. 2008.
[28] B. Cernuschi-Frias, "A combinatorial generalization of the stirling numbers of the second kind," in *Proc. ICECS. 8th IEEE Int. Conf. Electron., Circuits Syst.*, vol. 2, Sep. 2001, pp. 593–596.
[29] D. Popescu, F. Stoican, G. Stamatescu, L. Ichim, and C. Dragana, "Advanced UAV–WSN system for intelligent monitoring in precision agriculture," *Sensors*, vol. 20, no. 3, p. 817, Feb. 2020.
[30] S. Rashed and M. Soyturk, "Effects of UAV mobility patterns on data collection in wireless sensor networks," in *Proc. IEEE Int. Conf. Commun., Netw. Satell. (COMNESTAT)*, Dec. 2015, pp. 74–79.
[31] M. Dorigo, V. Maniezzo, and A. Colorni, "Ant system: Optimization by a colony of cooperating agents," *IEEE Trans. Syst., Man, Cybern. B. Cybern.*, vol. 26, no. 1, pp. 29–41, Feb. 1996.
[32] T. Lavoie and E. Merlo, "An accurate estimation of the Levenshtein distance using metric trees and Manhattan distance," in *Proc. 6th Int. Workshop Softw. Clones (IWSC)*, Zürich, Switzerland, Jun. 2012, pp. 1–7.
[33] S. Liu, Z. Wei, Z. Guo, X. Yuan, and Z. Feng, "Performance analysis of UAVs assisted data collection in wireless sensor network," in *Proc. IEEE 87th Veh. Technol. Conf. (VTC Spring)*, Jun. 2018, pp. 1–5.

ZHIQING WEI (Member, IEEE) received the B.E. and Ph.D. degrees from the Beijing University of Posts and Telecommunications (BUPT), Beijing, China, in 2010 and 2015, respectively. He is currently an Associate Professor with BUPT. He has authored one book, three book chapters, and more than 50 articles. His research interests include performance analysis and optimization of intelligent machine networks. He received the Exemplary Reviewer from the WIRELESS COMMUNICATIONS LETTERS, in 2017, and the Best Paper Award from the WCSP, in 2018. He served as the Registration Co-Chair for the IEEE/CIC ICCC, in 2018, the Publication Co-Chair for the IEEE/CIC ICCC, in 2019, and the IEEE/CIC ICCC, in 2020.

QIAN CHEN is currently pursuing the master's degree with the Beijing University of Posts and Telecommunications (BUPT), China. Her research interests include performance analysis and protocol design of UAV networks, vehicular networks, and so on.

SHUHANG LIU graduated from the Beijing University of Posts and Telecommunications (BUPT), in 2019. She is currently with China Tower. Her research interests include performance analysis, resource allocation, and path planning of UAV networks.

HUICI WU (Member, IEEE) received the Ph.D. degree from the Beijing University of Posts and Telecommunications (BUPT), Beijing, China, in 2018. From 2016 to 2017, she visited the Broadband Communications Research (BBCR) Group, University of Waterloo, Waterloo, ON, Canada. She is currently an Assistant Professor with BUPT. Her research interests include wireless communications and networks, with current emphasis on the collaborative air-to-ground communication and wireless access security. She served as the Publication Co-Chair for APCC, in 2018. She also served as a Guest Editor for *Science China Information Sciences*.